Inorganic Chemistry

pubs.acs.org/IC

Article

Reduction Mechanisms of Anticancer Osmium(VI) Complexes Revealed by Atomic Telemetry and Theoretical Calculations

Gilles Berger,* Anna Wach, Jacinto Sá, and Jakub Szlachetko

Cite This: *Inorg. Chem.* 2021, 60, 6663−6671

Read Online

ACCESS | Metrics & More | Article Recommendations | Supporting Information

ABSTRACT: Resonant X-ray emission spectroscopy (RXES) has developed in the past decade as a powerful tool to probe the chemical state of a metal center and *in situ* study chemical reactions. We have used it to monitor spectral changes associated with the reduction of osmium(VI) nitrido complexes to the osmium(III) ammine state by the biologically relevant reducing agent, glutathione. RXES difference maps are consistent with the proposed DFT mechanism and the formation of two stable osmium(IV) intermediates, thereby supporting the overall pathway for the reduction of these high-valent anticancer metal complexes for which reduction by thiols within cells may be essential to the antiproliferative activity.

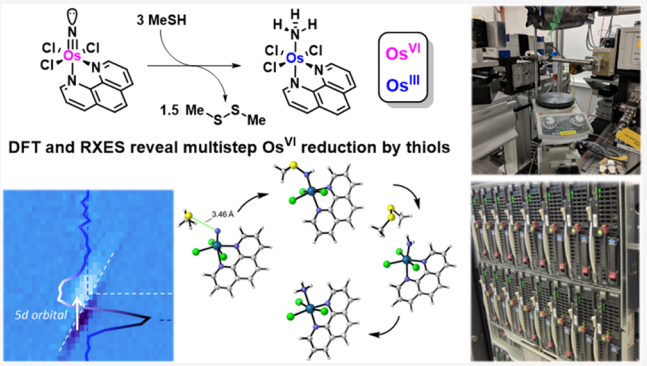

INTRODUCTION

Metal nitrides have been known since the mid-19th century[1] and span a various range of structures and reactivities.[2,3] Although these compounds have since driven interest for their structures and fundamental properties, only recently has emerged attention for their chemical reactivity and biological properties. The intriguing chemistry of late-transition metal nitrides attracted deep interest in the past years, and recent reports have shown their implication in a wide variety of organic transformations including C−H bond activation,[4−7] electrophilic reaction,[8−13] *N*−*N* coupling,[14−19] catalytic oxidation,[20−22] and nitrogen transfer.[23−29]

Osmium-based anticancer complexes exhibit encouraging activity with mechanisms of action that differ from current therapies.[30,31] Osmium(II) arene complexes containing azopyridine ligand derivatives have shown nanomolar-range activity toward a large assortment of cancer cell lines.[32] Similar types of osmium complexes have been proven to induce apoptosis and S-phase cell cycle arrest through a mitochondria-mediated process in A549 non-small cell lung cancer cells.[33] Osmium(II) half-sandwich complexes can react with glutathione (GSH) through ligand exchange and produce reactive oxygen species.[34] Such compounds have also been localized *in cellulo* using synchrotron-based X-ray fluorescence nanoprobes, highlighting their mitochondrial localization.[35]

The recently developed osmium(VI) nitrido complexes as used in the present study have been proven to be breast cancer stem cell-selective[36] and have shown promising effects on glioblastoma models.[37] The nitrido functionality demonstrated reactivity toward both nucleophiles and electrophiles, and it is likely that this reactive site is important for the biological activity of nitrido complexes. For now, little mechanistic information about the chemical properties that bring the anticancer activity of nitrido compounds is known. However, we believe that osmium(VI) can readily be reduced to lower oxidation state species in the presence of bionucleophiles and reducing agents like GSH, generating free radicals in the process and participating in the antiproliferation properties.

In the 70s, Eisenberger et al.[38] showed that synchrotron radiation can be used to observe characteristic radiation narrower than the lifetime width at the Cu K-edge. Later, Hämäläinen et al.[39] obtained high-resolution X-ray absorption spectra by using high-energy-resolution X-ray spectrometers combined with monochromatic beam excitation. Since then, many authors have explored the potential of high-energy-resolution X-ray spectrometers to obtain 2D-RXES (two-dimensional resonant X-ray emission spectroscopy) planes.[40,41] RXES, also known in the literature as resonant inelastic X-ray scattering (RIXS), is a photon-in photon-out X-ray spectroscopy capable of mapping the electronic structure of matter[42,43] in chemical[44,45] and biological systems.[46,47] The RXES process is based on the excitation of a core electron into unoccupied states and inner- or valence-shell electrons that are de-excited from the occupied states to the core levels, which leads to the emission of an X-ray photon. RXES relies on the intensities and energies of

Received: February 15, 2021
Published: April 19, 2021

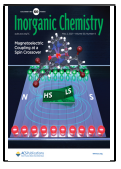

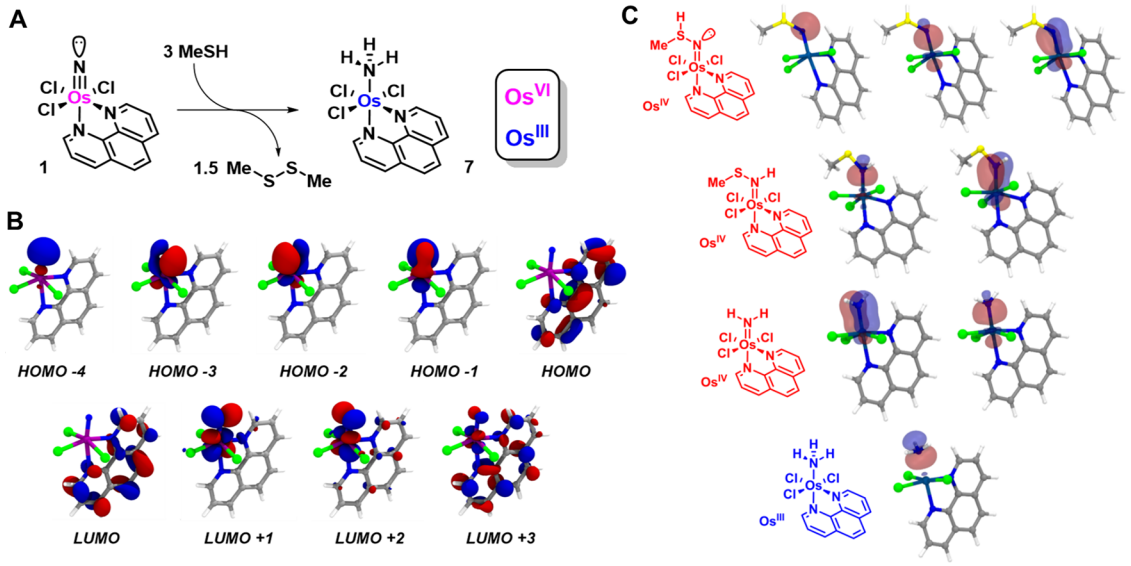

Figure 1. (A) Reduction of the osmium(VI) nitrido $OsNCl_3(phen)$ complex **1** to the osmium(III) ammine **7** by 3 equiv of methanethiol. (B) Localized frontier orbitals of complex **1**, showing the triple bonding of the nitrido, the ligand character of the HOMO and LUMO, and the Os−N π^* antibonding nature of the LUMO +1/+2, while LUMO +3 is spread over the entire molecule. (C) Natural bonding orbitals of the osmium(IV) intermediates **2**, **3**, and **6** and the final ammine complex **7**.

the incoming and emitted X-rays, allowing unoccupied and occupied electronic states of the metal to be probed with element specificity. The energy resolution of RXES, as compared to standard XAS (X-ray absorption spectroscopy), is not limited by the core-hole lifetime due to the superposition of photon absorption and emission processes. This is important for heavy elements such as 5d metals (i.e., osmium) carried out at the L_3 absorption edge and by detection of the Lα emission line. The L_3 core-hole broadening for heavy elements is in the order of a coupleeV, which makes detailed electronic structures difficult to obtain with conventional XAS methods. In the case of high energy resolution, the effect of core-hole broadening is reduced and the total energy resolution is defined by the spectrometer resolution, being in the order of 1 eV. Lomachenko et al.[48] compared RIXS and HERFD XANES (high-energy-resolution fluorescence detection X-ray absorption near-edge structure) spectroscopies for electronic and structural characterization of osmium compounds and showed that, in comparison to the conventional (total fluorescence yield) XANES, the high-resolution X-ray absorption spectrum is more informative, the peaks being sharper and fully resolved. RXES can therefore reveal fine changes in the electronic configuration of a 5d metal center with respect to small modifications on the ligand, allowing *in situ* chemical speciation at concentrations relatable to drug applications. It should be emphasized here that the L_3-edge spectroscopy is more sensitive to the chemical surrounding of the 5d metal center than K-edge measurements.[49,50]

The label-free method, termed atomic telemetry, has proved useful to study the interactions between metal complexes and biomolecules without the need for extraction, crystallization, and/or preconcentration.[47,51−54] The metal atom in the complex is directly affected by the chemical transformations, these being reflected in its electronic levels and subsequently transmitted through the interaction with the X-ray radiation, which is analogous to the radio telemetry. Atomic telemetry can detect and analyze low amounts of metals, making it a valuable method for elucidating the chemical fate of a metal center, as the geometry, oxidation state, and coordination sphere of the metal will be reflected in the X-ray absorption and emission spectra. X-ray photon-in photon-out core-level spectroscopy is therefore a powerful tool to map the electronic structure with time resolution and elemental specificity and under relevant conditions due to the high penetration of hard X-rays.[55,56] The method is especially suitable for complex and multi-elemental environments because the electronic structure is provided exclusively from the perspective of the investigated metal center of the molecule. We herein demonstrate its ability to provide critical structural data during a multistep reaction between an anticancer metal complex and a bionucleophile, supporting a DFT-established pathway.

As part of the investigation in both the biological properties of such metal nitrides and the chemical properties that would convey their anticancer activity, we thus report the use of real-time atomic telemetry to help confirm the anticipated DFT pathway for the reduction of osmium(VI) nitrido anticancer complexes by thiols as a multistep reduction from the VI to the III oxidation state with osmium(IV) intermediates (Figure 1). We used hard X-rays (∼10 keV) from the SuperXAS beamline of the Swiss Light Source synchrotron to follow the reduction of the atom center and the changes in its first coordination sphere.

RESULTS AND DISCUSSION

The nitrido ligand can display electrophilic to nucleophilic behavior, depending on the metal center and its ligands.[3] Osmium(VI) nitrido and other metal nitrides are known to undergo nucleophilic addition on their nitride with alkenes, amines, phosphines, and thiols.[12,13,57−60] The latter may be involved in the anticancer effects of this class of compounds by depleting GSH levels and reacting with thiolated proteins, giving rise to the unfolded protein response.[36] A careful examination of the reactivity of a (salen)ruthenium(VI) nitrido complex with thiols has been reported a couple of years ago.[61] We thus started by theoretically delineating the reaction mechanism of the osmium(VI) nitrido complex $OsNCl_3(phen)$ with the simplest organic thiol (namely, methanethiol) for obvious computational reasons, helped by key experimental facts from the similar

https://doi.org/10.1021/acs.inorgchem.1c00467
Inorg. Chem. 2021, 60, 6663−6671

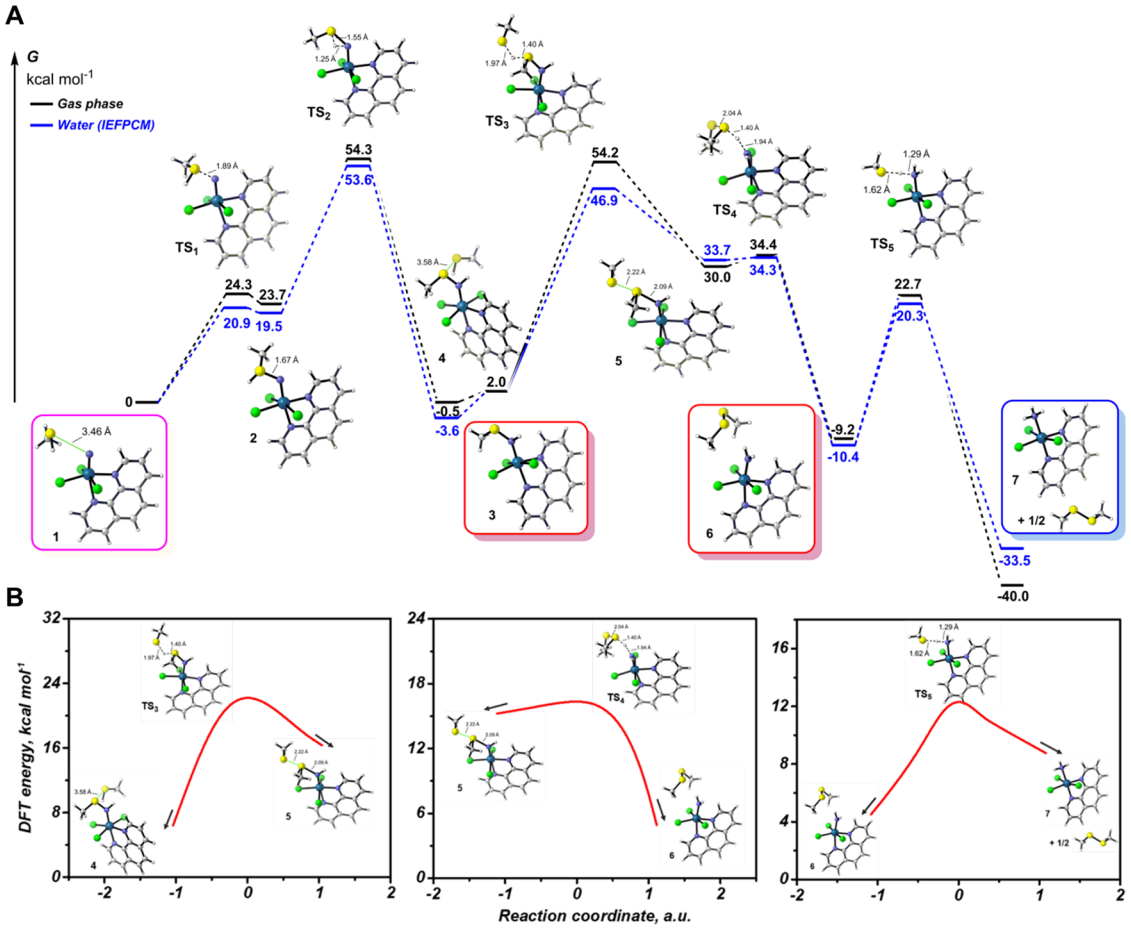

Figure 2. (A) DFT-predicted reaction pathway for the reduction of the osmium(VI) nitrido complex **1** with methanethiol. (B) IRC minimum energy pathways for $\mathbf{TS_3}$, $\mathbf{TS_4}$, and $\mathbf{TS_5}$.

reaction involving a ruthenium(VI) nitride.[61] These were as follows: (i) a sulfimido intermediate is produced after consumption of stoichiometric amounts of the thiol and (ii) addition of two more equivalents of the thiol led to the production of 1.5 equiv of the corresponding disulfide and the ruthenium(III) ammine through a sulfilamido intermediate. From there and consistently to these experimental findings, we aimed at locating all the transition states along that reaction pathway at the spin-unrestricted and dispersion-corrected density functional theory level (ωB97x-D/def2-TZVP, see the Experimental Section for full details).

The reaction sequence starts with the addition of the thiol to the nitride through a first transition state **TS1** that closely resembles the N−S adduct intermediate **2** (Figure 2). The latter will undergo proton shifting (**TS2**) to produce the first stable intermediate (**3**) after reaction with one thiol equivalent. In the case of ruthenium, available data suggest that the nucleophilic addition is the rate-limiting step instead of the proton transfer. Here, the activation energy is rather similar between both steps (24 vs 30 kcal mol^{-1}), although slightly higher for the proton shift. The sulfilamido osmium(IV) intermediate **3**, for which both an osmium and a ruthenium congener have been evidenced by X-ray crystallography,[11,61] then reacts with a second equivalent of thiol through a rate-limiting addition. Proton transfer to the sulfilamido moiety forms the short-lived intermediate **5**, and the rapid proton shifting to the nitrogen will expel one disulfide equivalent and produce the osmium(IV) imido species **6**. We can see that the proton transfer steps can involve rather high energy barriers (**TS2** and **TS3**), suggesting that proton shuttling through a water molecule may facilitate the reaction. A last hydrogen transfer step (**TS5**), consuming the third thiol equivalent, will finally deliver the osmium(III) ammine complex and bring the overall thermodynamic driving force to the reaction. Apart from transition states leading to the formation of **3**, the stationary saddle points **TS3**, **TS4**, and **TS5** are not obvious and were verified as the actual transition structures of the considered steps by following the minimal energy pathway and integration of the intrinsic reaction coordinate (IRC, Figure 2B), showing that they indeed connect the expected reactants and products.

We then turned to atomic telemetry and resonant X-ray emission spectroscopy (RXES) to validate these theoretical predictions and follow the multistep reduction of Os^{VI} to Os^{III} through Os^{IV} intermediates. The reaction pathway was elucidated by analyzing the changes in RXES maps (ΔRXES) in real time during the reaction with the bionucleophile GSH, suspected to be involved in the antiproliferative activity of these high-valent nitrido complexes (Figure 3). The RXES difference maps (ΔRXES), which reflect relative changes in the density of occupied and unoccupied electronic states, were obtained by direct subtraction of normalized RXES planes for the corresponding Os complexes. The individual RXES maps can be found in the Supporting Information (Figure S3). It should be noted that direct differential maps were obtained by the use of a dispersive von Hamos spectrometer, enabling precise correction of the incoming energy.

https://doi.org/10.1021/acs.inorgchem.1c00467
Inorg. Chem. 2021, 60, 6663−6671

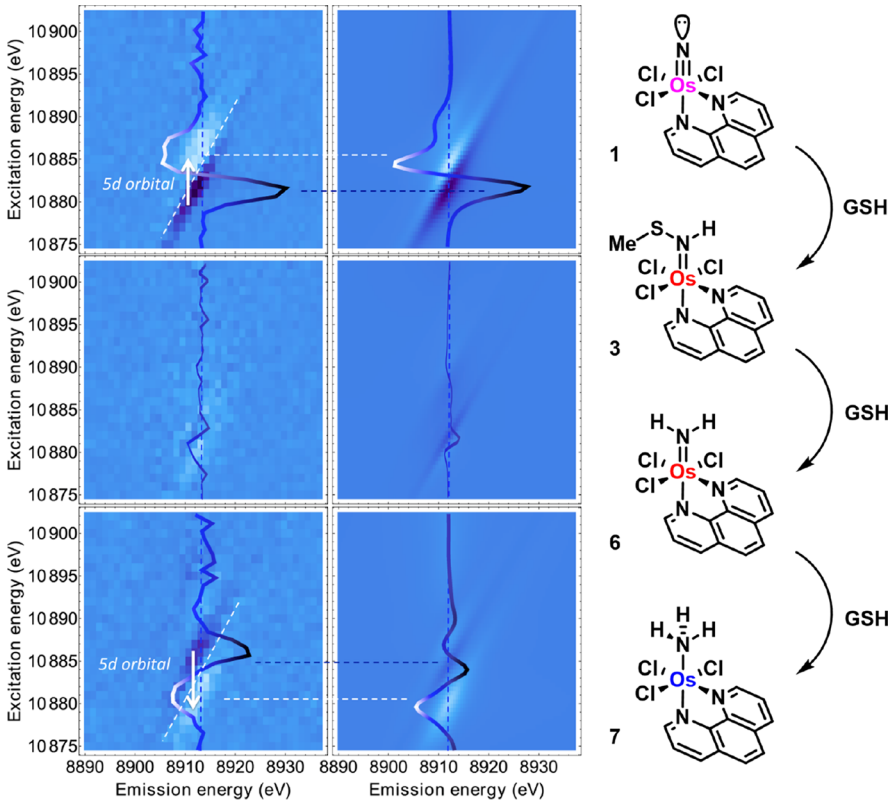

Figure 3. ΔRXES maps revealing the electronic changes induced by sequential addition of 3 equiv of GSH. The plots show the differences in the electronic states when going from complex **1** to complex **3** (top, $\Delta RXES = RXES_3 - RXES_1$); complex **3** to complex **6** (middle, $\Delta RXES = RXES_6 - RXES_3$); and complex **6** to a 50:50 mixture of **6** and **7** (bottom, $\Delta RXES = (1/2\ RXES_7 + 1/2\ RXES_6) - RXES_6$). The left and right plots, respectively, show the experimental and theoretical ΔRXES maps. The position of $2p_{3/2} \rightarrow 5d$ resonance indicating changes in the occupancy of 5d states is marked with a dashed line. The direction of changes in the energy position of 5d orbitals is marked with a white arrow.

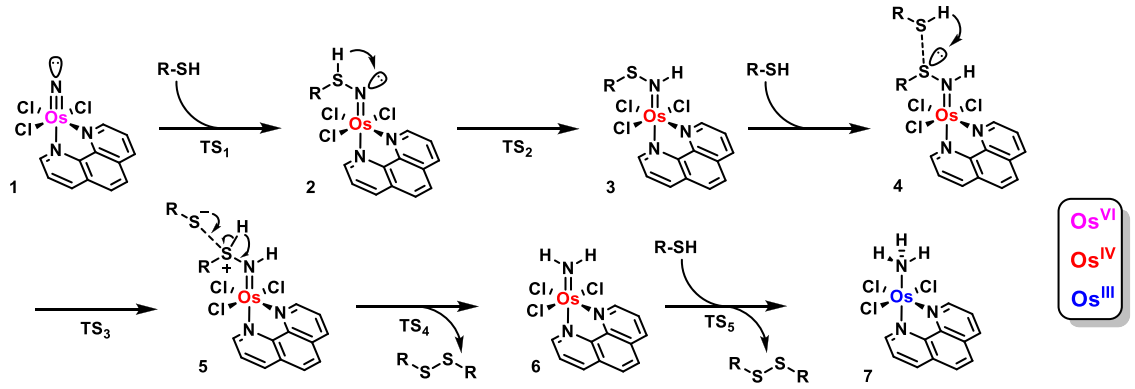

Figure 4. Proposed reaction mechanism for the reduction of osmium(VI) nitrido complexes by thiols. Oxidation states were determined using localized orbital bonding analysis as implemented in the Q-Chem code.[62]

The addition of the first equivalent of GSH caused a significant change in the electronic structure around the metal center. This translated in the ΔRXES maps as a clear shift of the main resonance toward higher energies, contrasting with the intuitively expected change when increasing the electron density and lowering the oxidation state. The experimental ΔRXES profile is, however, well reproduced by the induced change in the theoretical density of electronic states for the optimized structures **1** and **3**. These results confirm that **3** is formed after the first addition of the thiol and that this first step appears to occur stoichiometrically and to completion. The apparent contradiction in the energy shift direction is explained by a significant reorganization of the Os 5d unoccupied orbital as a result of the structural transformation in the second coordination shell and the associated changes in the bond length between Os and N atoms. Additionally, the strength of hybridization between Os d and N p orbitals is lower in the Os(IV) complex and influences the strength of the resonance between $2p_{3/2}$ and unoccupied states.

The addition of the second equivalent of GSH resulted in minor changes to the ΔRXES map, which suggests changes in the second coordination sphere of the Os complex but not in its oxidation state. This is in agreement with the DFT mechanism, in which the reaction of complex **3** with the second thiol molecule forms complex **6**, which only differs from its predecessor by the coordinated ligands to the Os-bound

https://doi.org/10.1021/acs.inorgchem.1c00467
Inorg. Chem. 2021, 60, 6663−6671

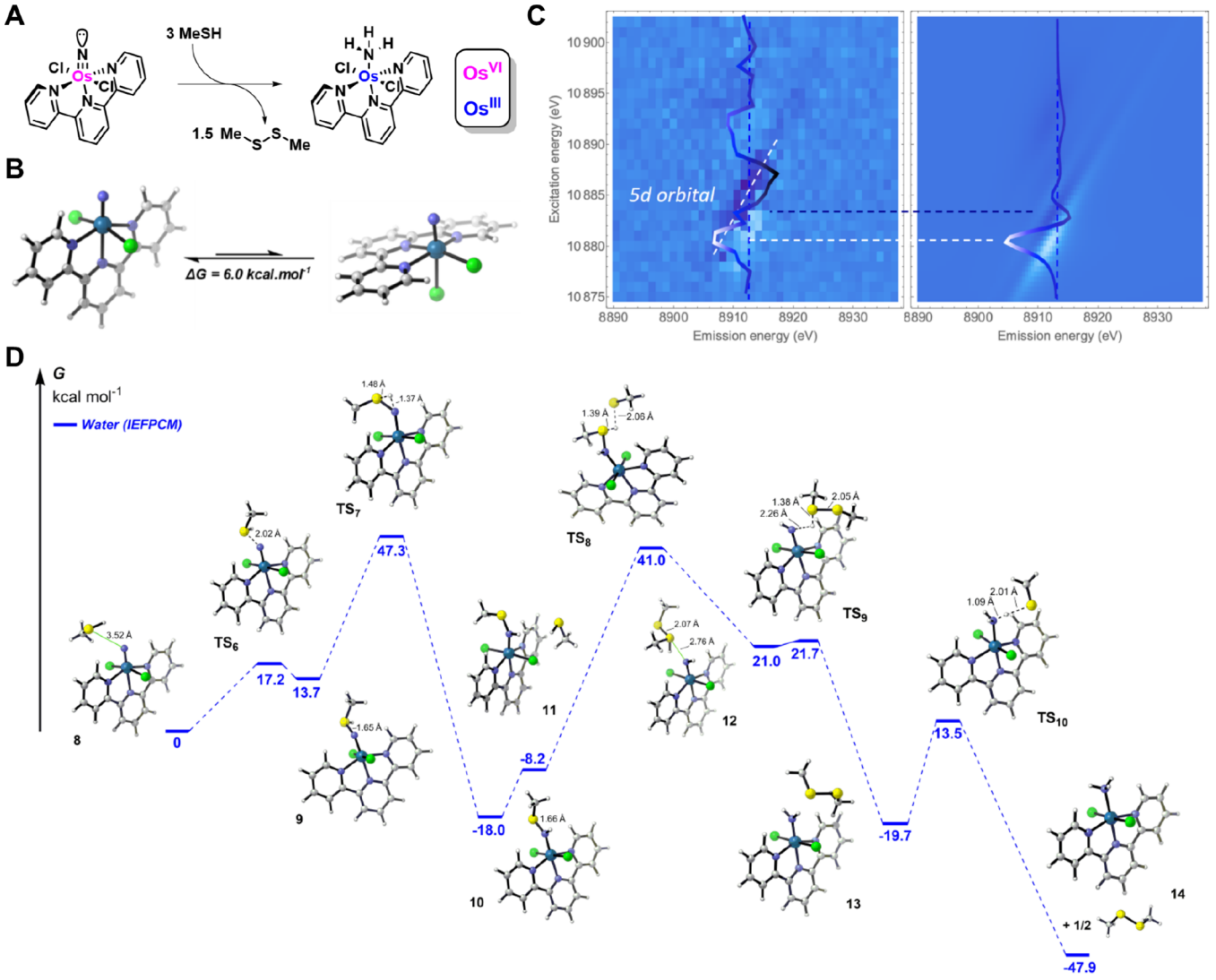

Figure 5. (A) Reduction of the cationic terpyridine complex **8** from the osmium(VI) nitrido to the osmium(III) ammine **14** by three molecules of methanethiol. (B) Axial-equatorial isomerization of complex **8**, with a 6 kcal mol^{-1} free energy gap in favor of the axial isomer. (C) ΔRXES maps between the final and initial states (ΔRXES = $RXES_{14} - RXES_{8}$). (D) DFT-computed pathway for the multistep reduction of **8** by methanethiol.

nitrogen. These small spectral changes from the sulfilamido osmium(IV) intermediate to the imido osmium(IV) are well reproduced using the complete transformation of complex **3** into **6**, i.e., stoichiometric formation of complex **6**. However, these are too small to unequivocally confirm the presence of both **3** and **6**, but rather confirm the *in situ* generation of osmium(IV) intermediates, for which the structures are postulated by DFT.

The final addition of GSH caused a significant alteration in and around the main resonance, which is consistent with a change in the oxidation state. Theoretical analysis of these differences revealed interesting conclusions. First, the observed resonant X-ray emission spectral changes confirmed the formation of the final ammine osmium(III) complex **7** as the product of the reaction. The shift of the 5d resonance toward lower energies confirms the reduction from the oxidation state IV to III. Semiquantitative analysis of the ΔRXES maps further showed that this third step of the sequential reaction did not reach completion. Around 50% of the osmium(III) ammine **7** is produced at the end of the experiment, and this incomplete reaction may be due to our experimental setup, the inability to run the reaction in a controlled atmosphere, or the limited amount of time available at the beam to allow the reaction to complete. Based on our DFT predictions and experimental ΔRXES maps, we therefore propose the multistep reaction mechanism depicted in Figure 4, for the reduction of osmium(VI) nitrido anticancer complexes by thiols and GSH within cells. The reaction involves five consecutive steps and three stable intermediates.

To verify our hypothesis, we have run the reaction with another complex that was also used as an anticancer agent against glioblastoma models. Here too, the addition of 3 equiv of GSH induced spectral changes that reflected the transformation to the final Os(III) ammine compound, confirming our data on the phenanthroline complex. In the terpyridine case, however, multiple simultaneous processes involving the isomerization of the starting nitrido compound between its equatorial and axial isomers rendered the interpretation of the spectral changes associated with the intermediate Os(IV) states difficult but still confirmed the reduction of the Os(III) state and the ammine complex **14** (Figure 5).

https://doi.org/10.1021/acs.inorgchem.1c00467
Inorg. Chem. 2021, 60, 6663−6671

CONCLUSIONS

To summarize, we disclose here the first use of real-time atomic telemetry for a multistep reaction involving a metal complex and, guided by DFT, uncovered the reaction mechanism. We were able to follow the reduction of osmium(VI) nitrido complexes to osmium(III) ammine by thiols and more specifically by the biologically relevant GSH. This marks a new achievement for resonant X-ray emission spectroscopy in elucidating the relationship between the structure and mechanism of action for biological systems.

The past few decades witnessed the rapid development of X-ray sources and absorption techniques, and second-order spectroscopies can provide incomparable electronic and structural information on a wide variety of systems. XAS methods have been employed for many years to study the chemical state of samples, both *in situ* and *ex situ*. However, the high-energy-resolution spectroscopy methods push XAS-based techniques toward enhanced sensitivity, allowing observation of tiny chemical changes in the studied samples.[63,64] The use of hard X-ray facilities and the monitoring of real-time spectral changes while the reaction takes place represent an important accomplishment for both X-ray spectroscopy and the chemical reactivity of such metal nitrides, which also convey antiproliferative properties as anticancer compounds. Our theoretical work is validated by the RXES experiments, bringing experimental proof for the formation of the postulated osmium(IV) complexes as reaction intermediates. Changes in the collected emission maps match the predicted spectra of these intermediates, and our study highlights the feasibility of the concept, opening the way for the use of X-ray spectroscopy to investigate complex reaction mechanisms.

EXPERIMENTAL SECTION

Synthesis of the Osmium Complexes. The complexes were prepared following previously published procedures.[65,66] Briefly, a tetrabutylammonium salt of the Os(VI) nitrido chloride was first produced followed by the complexation with the bi- and tridentate heterocyclic ligands in organic solvents, affording the desired compounds by precipitation over the course of the reaction. These were then filtered off and washed thoroughly with the reaction solvent.

Real-Time Atomic Telemetry. The electronic structure of osmium was investigated by means of resonant X-ray emission spectroscopy at the SuperXAS beamline of the Swiss Light Source synchrotron at Paul Scherrer Institute, Switzerland. The incidence X-ray energy was monochromatized with double-crystal Si(111) and tuned around the L_3 edge of Os. The incident photon energy was calibrated to the copper metal K absorption edge energy using a reference value of 8979 eV. The obtained inflection point of the edge for the Os(VI) complex at an energy of 10881.2 eV is in agreement with previously reported data for Os(IV) (10879.6 eV) and Os(V) (10880.1 eV) complexes.[67] Use of L_3-edge spectroscopy ($2p_{3/2}$ atomic level) provides direct dipole $2p_{3/2}$ excitation to the unoccupied 5d orbital. The following $3d \rightarrow 2p_{3/2}$ electronic decay and accompanying Lα X-ray emission at 8911.7 eV were monitored using a high-energy-resolution X-ray spectrometer setup.[41,68] The setup compromise a 25 cm-radius Si(444) diffraction crystal and 2D Pilatus detector. The experimental resolution, including the incidence beam, was determined to be around 2 eV, a value significantly lower than that of the natural broadening of the L_3 core hole of 5.1 eV.

A 12.5 mM solution of the starting osmium(VI) complex in 4 mL of DMSO was sequentially added with GSH as concentrated water solutions (100 μL for each, 300 μL total), 1 equiv at a time, and spectral changes were monitored. Each equivalent was added after a steady state was reached, and the timeline was as follows: 1.5 h of RXES measurement, then addition of the next equivalent of the thiol, 1 h of reaction, and then again 1.5 h of measurement, with this sequence being repeated to the last step. For the terpyridine complex, the RXES measurements were shortened to 1 h, and the second and third equivalents were added together. The sample was enclosed within a custom-made cell equipped with a Kapton window ensuring sufficient X-ray transmission for incidence and emitted X-rays. The RXES planes were collected continuously around the osmium L_3 absorption edge with an acquisition time of 200 s per full map. Typically, we recorded four full maps at one sample position and a total of six to eight points were acquired during each reaction steps. This procedure allows reduction of radiation damage, and a constant circulation of the solution was ensured using a magnetic stirrer.

X-ray Data Analysis and Simulation. The collected 2D-RXES data were normalized employing conventional procedures. The 2D background function was first determined in a fitting procedure at incident and emission energies where no fluorescence was detected. This background function was then removed from the corresponding RXES maps. Then, for the highest incidence energies, the maximum XES signal was normalized to 1 so that the projected high-energy-resolution XAS (HR-XAS) function from the RXES plane was normalized to 0−1 values at below and above edge energies, respectively. The HR-XAS spectra (shown in the Supporting Information) were obtained by cutting the RXES planes across the most intense emission energy (i.e., Lα_1 peak maximum at 8911.7 eV). The theoretical resonant X-ray emission spectra were calculated with the second-order perturbation theorem. The differential cross-sectional equations developed by Tulkki and Aberg[69] were employed for the calculation of X-ray emission signals at given incidence energies. The energies of the initial and final states were taken from Deslattes et al.,[70] and the corresponding core-hole lifetimes were taken from Campbell and Papp.[71] The oscillator strength function for excitation channels was approximated by electronic density of states calculated with the FEFF 9.6 program, a self-consistent multiple-scattering code.[72] DFT-optimized geometries were used as inputs for FEFF calculations.

Quantum Mechanical Methods. All quantum mechanical calculations have been achieved using Gaussian09 rev D.01, Orca 4.0.1,[73] and Q-Chem 4.6. Geometries of the investigated systems were fully optimized at the spin-unrestricted density functional theory level using the dispersion-corrected ωB97x-D exchange−correlation functional.[74] The balanced polarized triple-zeta basis set def2-TZVP from Ahlrichs and Weigend[75,76] has been used for all atoms, except for the metal, for which either the quasi-relativistic Stuttgart−Dresden core potential was used[4] or, for a sharper description of relativistic effects for core electrons, an all-electron scalar relativistic approximation (zeroth-order regular approximation, ZORA)[77] as implemented in ORCA 4. Potential energy surface minima found upon optimization were confirmed by frequency calculations, and free energies were corrected to account for the zero-point energy. Optimized geometries were verified as minima (i.e., zero imaginary frequencies). The synchronous transit-guided quasi-Newton method[78,79] was used for locating transition structures. These structures were further verified as saddle points by frequency calculations (i.e., one and only one imaginary frequency). The bulk solvent effects for water have been included through the integral equation formalism version of the polarizable continuum model.[80] Natural bond orbital analysis was performed using the latest version of the program from Weinhold and co-workers (NBOPro 6.0).[81]

ASSOCIATED CONTENT

Supporting Information

The Supporting Information is available free of charge at https://pubs.acs.org/doi/10.1021/acs.inorgchem.1c00467.

DFT-optimized geometries, additional spectral data, and NMR spectra of the osmium(VI) complexes (PDF)

AUTHOR INFORMATION

Corresponding Author

Gilles Berger − *Microbiology, Bioorganic & Macromolecular Chemistry, Faculty of Pharmacy, Université Libre de Bruxelles,*

https://doi.org/10.1021/acs.inorgchem.1c00467
Inorg. Chem. 2021, 60, 6663−6671

1050 Brussels, Belgium; Harvey Cushing Neuro-Oncology Laboratories, Department of Neurosurgery, Brigham and Women's Hospital, Harvard Medical School, Boston, Massachusetts 02115, United States; Department of Chemistry, Massachusetts Institute of Technology, Cambridge, Massachusetts 02139, United States; orcid.org/0000-0002-5418-9107; Email: gilles.berger@ulb.be

Authors

Anna Wach − *Institute of Nuclear Physics, Polish Academy of Sciences, 31342 Krakow, Poland;* orcid.org/0000-0003-3112-2759

Jacinto Sá − *Institute of Physical Chemistry, Polish Academy of Sciences, 01-224 Warsaw, Poland; Physical Chemistry Division, Department of Chemistry, Ångström Laboratory, Uppsala University, 75120 Uppsala, Sweden;* orcid.org/0000-0003-2124-9510

Jakub Szlachetko − *Institute of Nuclear Physics, Polish Academy of Sciences, 31342 Krakow, Poland;* orcid.org/0000-0002-7526-3097

Complete contact information is available at: https://pubs.acs.org/10.1021/acs.inorgchem.1c00467

Author Contributions

G.B. performed the chemical synthesis of the compounds and all DFT calculations and participated in the experiments at the SLS synchrotron. He prepared the manuscript and analyzed the data. A.W. conducted the experiments at the SLS and participated in the data analysis. J.Sà contributed to the design of the study and data analysis. J.Szlachetko participated in the experiments at the SLS and analyzed the data.

Notes

The authors declare no competing financial interest.

■ ACKNOWLEDGMENTS

Authors would like to acknowledge the Swiss Light Source for access to the SuperXAS beamline. G.B. was a recipient of an FRS-FNRS Award. J.S. acknowledges partial support from the National Science Center in Poland under grant 2016/21/D/ST4/00378.

■ REFERENCES

(1) Fritzsche, J.; Struve, H. Ueber Die Osman-Osmiumsäure. *J. Prakt. Chem.* **1847**, *41*, 97−113.
(2) Eikey, R. A.; Abu-Omar, M. M. Nitrido and Imido Transition Metal Complexes of Groups 6-8. *Coord. Chem. Rev.* **2003**, *243*, 83−124.
(3) Smith, J. M. Reactive Transition Metal Nitride Complexes. *Prog. Inorg. Chem.* **2014**, *58*, 417−470.
(4) Schlangen, M.; Neugebauer, J.; Reiher, M.; Schröder, D.; López, J. P.; Haryono, M.; Heinemann, F. W.; Grohmann, A.; Schwarz, H. Gas-Phase C-H and N-H Bond Activation by a High Valent Nitrido-Iron Dication and ⟨NH⟩-Transfer to Activated Olefins. *J. Am. Chem. Soc.* **2008**, *130*, 4285−4294.
(5) Musch Long, A. K.; Yu, R. P.; Timmer, G. H.; Berry, J. F. Aryl C-H Bond Amination by an Electrophilic Diruthenium Nitride. *J. Am. Chem. Soc.* **2010**, *132*, 12228−12230.
(6) Carmen, C.; Atienza, H.; Bowman, A. C.; Lobkovsky, E.; Chirik, P. J. Photolysis and Thermolysis of Bis (Imino) Pyridine Cobalt Azides : C-H Activation from Putative Coablt Nitrido Complexes. *J. Am. Chem. Soc.* **2010**, *132*, 16343−16345.
(7) Thomson, R. K.; Cantat, T.; Scott, B. L.; Morris, D. E.; Batista, E. R.; Kiplinger, J. L. Uranium Azide Photolysis Results in C−H Bond Activation and Provides Evidence for a Terminal Uranium Nitride. *Nat. Chem.* **2010**, *2*, 723−729.
(8) Meyer, T. J.; Huynh, M. H. V. The Remarkable Reactivity of High Oxidation State Ruthenium and Osmium Polypyridyl Complexes. *Inorg. Chem.* **2003**, *42*, 8140−8160.
(9) Huynh, M. H. V.; Meyer, T. J.; Labouriau, A.; Morris, D. E.; White, P. S. Multiple Mixed-Valence Behavior in Reaction between Trans- [Os VI (Tpy)(Cl) 2 (N)] + and NH 3. *J. Am. Chem. Soc.* **2003**, *125*, 2828−2829.
(10) Huynh, M. H. V.; White, P. S.; Carter, C. A.; Meyer, T. J. Formation and Reactivity of the Osmium(IV)-Cyanoimido Complex [OsIV(Bpy)(Cl)3(NCN)]. *Angew. Chem., Int. Ed.* **2001**, *40*, 3037−3039.
(11) Huynh, M. H. V.; El-Samanody, E. S.; Demadis, K. D.; White, P. S.; Meyer, T. J. Mechanism and Molecular-Electronic Structure Correlations in a Novel Series of Osmium(V) Hydrazido Complexes. *Inorg. Chem.* **2000**, *39*, 3075−3085.
(12) Man, W. L.; Xie, J.; Lo, P. K.; Lam, W. W. Y.; Yiu, S. M.; Lau, K. C.; Lau, T. C. Functionalization of Alkynes by a (Salen)Ruthenium(VI) Nitrido Complex. *Angew. Chem.,Int. Ed.* **2014**, *53*, 8463−8466.
(13) Huynh, M. H. V.; Baker, R. T.; Jameson, D. L.; Labouriau, A.; Meyer, T. J. Formation and Reactivity of the Osmium(IV)-Azidoimido Complex, PPN[OsVI(Bpy)(Cl)3(N4)]. *J. Am. Chem. Soc.* **2002**, *124*, 4580−4582.
(14) Ware, D. C.; Taube, H. Substitution-Induced Nitrogen-Nitrogen Coupling for Nitride Coordinated to Osmium(Vi). *Inorg. Chem.* **1991**, *30*, 4605−4610.
(15) Seymore, S. B.; Brown, S. N. Polar Effects in Nitride Coupling Reactions. *Inorg. Chem.* **2002**, *41*, 462−469.
(16) Man, W. L.; Tang, T. M.; Wong, T. W.; Lau, T. C.; Peng, S. M.; Wong, W. T. Highly Electrophilic (Salen)Ruthenium(VI) Nitrido Complexes. *J. Am. Chem. Soc.* **2004**, *126*, 478−479.
(17) Yiu, S. M.; Lam, W. W. Y.; Ho, C. M.; Lau, T. C. Facile N···N Coupling of Manganese(V) Imido Species. *J. Am. Chem. Soc.* **2007**, *129*, 803−809.
(18) Man, W.-L.; Kwong, H.-K.; Lam, W. W. Y.; Xiang, J.; Wong, T.-W.; Lam, W.-H.; Wong, W.-T.; Peng, S.-M.; Lau, T.-C. General Synthesis of (Salen) Ruthenium (III) Complexes via N··· N Coupling of (Salen) Ruthenium (VI) Nitrides. *Inorg. Chem.* **2008**, *47*, 5936−5944.
(19) Man, W.-L.; Chen, G.; Yiu, S.-M.; Shek, L.; Wong, W.-Y.; Wong, W.-T.; Lau, T.-C. Formation of [Small Mu]-Dinitrogen (Salen) Osmium Complexes via Ligand-Induced N N Coupling of (Salen)-Osmium(vi) Nitrides. *Dalt. Trans.* **2010**, *39*, 11163−11170.
(20) Bendix, J.; Meyer, K.; Weyhermüller, T.; Bill, E.; Metzler-Nolte, N.; Wieghardt, K. Nitridocyanometalates of Cr V , Mn V , and Mn VI †. *Inorg. Chem.* **1998**, *37*, 1767−1775.
(21) Yiu, S. M.; Wu, Z. B.; Mak, C. K.; Lau, T. C. FeCl3-Activated Oxidation of Alkanes by [Os(N)O 3]. *J. Am. Chem. Soc.* **2004**, *126*, 14921−14929.
(22) Kwong, H.-K.; Lo, P.-K.; Lau, K.-C.; Lau, T.-C. Epoxidation of Alkenes and Oxidation of Alcohols with Hydrogen Peroxide Catalyzed by a Manganese(v) Nitrido Complex. *Chem. Commun.* **2011**, *47*, 4273−4275.
(23) Groves, J. T.; Takahashi, T. Activation and Transfer of Nitrogen from a Nitridomanganese(V) Porphyrin Complex. Aza Analog of Epoxidation. *J. Am. Chem. Soc.* **1983**, *105*, 2073−2074.
(24) Du Bois, J.; Tomooka, C. S.; Hong, J.; Carreira, E. M. Nitridomanganese(V) Complexes: Design, Preparation, and Use as Nitrogen Atom-Transfer Reagents. *Acc. Chem. Res.* **1997**, *30*, 364−372.
(25) Curley, J. J.; Sceats, E. L.; Cummins, C. C. A Cycle for Organic Nitrile Synthesis via Dinitrogen Cleavage. *J. Am. Chem. Soc.* **2006**, *128*, 14036−14037.
(26) Figueroa, J. S.; Piro, N. A.; Clough, C. R.; Cummins, C. C. A Nitridoniobium(V) Reagent That Effects Acid Chloride to Organic Nitrile Conversion: Synthesis via Heterodinuclear (Nb/Mo) Dinitrogen Cleavage, Mechanistic Insights, and Recycling. *J. Am. Chem. Soc.* **2006**, *128*, 940−950.
(27) Watanabe, D.; Gondo, S.; Seino, H.; Mizobe, Y. N-N Bond Cleavage of Organohydrazines by Molybdenum(II) and Tungsten(II) Complexes Containing a Linear Tetraphosphine Ligand. Formation of

Nitrido or Imido Complexes and Their Reactivities. *Organometallics* **2007**, *26*, 4909−4920.
(28) Sarkar, S.; Abboud, K. A.; Veige, A. S. Addition of Mild Electrophiles to a Mo≡N Triple Bond and Nitrile Synthesis via Metal-Mediated N-Atom Transfer to Acid Chlorides. *J. Am. Chem. Soc.* **2008**, *130*, 16128−16129.
(29) Xiang, J.; Jin, X.-X.; Su, Q.-Q.; Cheng, S.-C.; Ko, C.-C.; Man, W.-L.; Xue, M.; Wu, L.; Che, C.-M.; Lau, T.-C. Photochemical Nitrogenation of Alkanes and Arenes by a Strongly Luminescent Osmium(VI) Nitrido Complex. *Commun. Chem.* **2019**, *2*, 40.
(30) van Rijt, S. H.; Peacock, A. F. A.; Johnstone, R. D. L.; Parsons, S.; Sadler, P. J. Organometallic Osmium(II) Arene Anticancer Complexes Containing Picolinate Derivatives. *Inorg. Chem.* **2009**, *48*, 1753−1762.
(31) Kostrhunova, H.; Florian, J.; Novakova, O.; Peacock, A. F. a.; Sadler, P. J.; Brabec, V. DNA Interactions of Monofunctional Organometallic Osmium(II) Antitumor Complexes in Cell-Free Media. *J. Med. Chem.* **2008**, *51*, 3635−3643.
(32) Fu, Y.; Habtemariam, A.; Pizarro, A. M.; van Rijt, S. H.; Healey, D. J.; Cooper, P. a.; Shnyder, S. D.; Clarkson, G. J.; Sadler, P. J. Organometallic Osmium Arene Complexes with Potent Cancer Cell Cytotoxicity. *J. Med. Chem.* **2010**, *53*, 8192−8196.
(33) van Rijt, S. H.; Romero-Canelón, I.; Fu, Y.; Shnyder, S. D.; Sadler, P. J. Potent Organometallic Osmium Compounds Induce Mitochondria-Mediated Apoptosis and S-Phase Cell Cycle Arrest in A549 Non-Small Cell Lung Cancer Cells. *Metallomics* **2014**, *6*, 1014−1022.
(34) Needham, R. J.; Sanchez-Cano, C.; Zhang, X.; Romero-Canelón, I.; Habtemariam, A.; Cooper, M. S.; Meszaros, L.; Clarkson, G. J.; Blower, P. J.; Sadler, P. J. In-Cell Activation of Organo-Osmium(II) Anticancer Complexes. *Angew. Chem., Int. Ed.* **2017**, *56*, 1017−1020.
(35) Sanchez-Cano, C.; Romero-Canelón, I.; Yang, Y.; Hands-Portman, I. J.; Bohic, S.; Cloetens, P.; Sadler, P. J. Synchrotron X-Ray Fluorescence Nanoprobe Reveals Target Sites for Organo-Osmium Complex in Human Ovarian Cancer Cells. *Chem. - A Eur. J.* **2017**, *23*, 2512−2516.
(36) Suntharalingam, K.; Lin, W.; Johnstone, T. C.; Bruno, P. M.; Zheng, Y.-R.; Hemann, M. T.; Lippard, S. J. A Breast Cancer Stem Cell-Selective, Mammospheres-Potent Osmium(VI) Nitrido Complex. *J. Am. Chem. Soc.* **2014**, *136*, 14413−14416.
(37) Berger, G.; Grauwet, K.; Zhang, H.; Hussey, A. M.; Nowicki, M. O.; Wang, D. I.; Chiocca, E. A.; Lawler, S. E.; Lippard, S. J. Anticancer Activity of Osmium (VI) Nitrido Complexes in Patient- Derived Glioblastoma Initiating Cells and in Vivo Mouse Models. *Cancer Lett.* **2018**, *416*, 138−148.
(38) Eisenberger, P.; Platzman, P. M.; Winick, H. X-Ray Resonant Raman Scattering: Observation of Characteristic Radiation Narrower than the Lifetime Width. *Phys. Rev. Lett.* **1976**, *36*, 623−626.
(39) Hämäläinen, K.; Siddons, D. P.; Hastings, J. B.; Berman, L. E. Elimination of the Inner-Shell Lifetime Broadening in X-Ray-Absorption Spectroscopy. *Phys. Rev. Lett.* **1991**, *67*, 2850−2853.
(40) Yan, J. J.; Kroll, T.; Baker, M. L.; Wilson, S. A.; Decréau, R.; Lundberg, M.; Sokaras, D.; Glatzel, P.; Hedman, B.; Hodgson, K. O.; Solomon, E. I. Resonant Inelastic X-Ray Scattering Determination of the Electronic Structure of Oxyhemoglobin and Its Model Complex. *Proc. Natl. Acad. Sci. U. S. A.* **2019**, *116*, 2854−2859.
(41) Szlachetko, J.; Sá, J.; Nachtegaal, M.; Hartfelder, U.; Dousse, J.-C.; Hoszowska, J.; Abreu Fernandes, D. L.; Shi, H.; Stampfl, C. Real Time Determination of the Electronic Structure of Unstable Reaction Intermediates during Au2O3 Reduction. *J. Phys. Chem. Lett.* **2014**, *5*, 80−84.
(42) De Groot, F. High-Resolution X-Ray Emission and X-Ray Absorption Spectroscopy. *Chem. Rev.* **2001**, *101*, 1779−1808.
(43) Glatzel, P.; Sikora, M.; Fernández-García, M. Resonant X-Ray Spectroscopy to Study K Absorption Pre-Edges in 3d Transition Metal Compounds. *Eur. Phys. J. Spec. Top.* **2009**, *169*, 207−214.
(44) Safonova, O. V.; Tromp, M.; Van Bokhoven, J. A.; De Groot, F. M. F.; Evans, J.; Glatzel, P. Identification of CO Adsorption Sites in Supported Pt Catalysts Using High-Energy-Resolution Fluorescence Detection X-Ray Spectroscopy. *J. Phys. Chem. B* **2006**, *110*, 16162−16164.
(45) Sá, J.; Szlachetko, J.; Sikora, M.; Kavčič, M.; Safonova, O. V.; Nachtegaal, M. Magnetic Manipulation of Molecules on a Non-Magnetic Catalytic Surface. *Nanoscale* **2013**, *5*, 8462−8465.
(46) Van Kuiken, B. E.; Hahn, A. W.; Nayyar, B.; Schiewer, C. E.; Lee, S. C.; Meyer, F.; Weyhermüller, T.; Nicolaou, A.; Cui, Y. T.; Miyawaki, J.; Harada, Y.; Debeer, S. Electronic Spectra of Iron-Sulfur Complexes Measured by 2p3d RIXS Spectroscopy. *Inorg. Chem.* **2018**, *57*, 7355−7361.
(47) Czapla-Masztafiak, J.; Nogueira, J. J.; Lipiec, E.; Kwiatek, W. M.; Wood, B. R.; Deacon, G. B.; Kayser, Y.; Fernandes, D. L. A.; Pavliuk, M. V.; Szlachetko, J.; González, L.; Sá, J. Direct Determination of Metal Complexes' Interaction with DNA by Atomic Telemetry and Multiscale Molecular Dynamics. *J. Phys. Chem. Lett.* **2017**, *8*, 805−811.
(48) Lomachenko, K. A.; Garino, C.; Gallo, E.; Gianolio, D.; Gobetto, R.; Glatzel, P.; Smolentsev, N.; Smolentsev, G.; Soldatov, A. V.; Lamberti, C.; Salassa, L. High Energy Resolution Core-Level X-Ray Spectroscopy for Electronic and Structural Characterization of Osmium Compounds. *Phys. Chem. Chem. Phys.* **2013**, *15*, 16152−16159.
(49) Baker, M. L.; Mara, M. W.; Yan, J. J.; Hodgson, K. O.; Hedman, B.; Solomon, E. I. K- and L-Edge X-Ray Absorption Spectroscopy (XAS) and Resonant Inelastic X-Ray Scattering (RIXS) Determination of Differential Orbital Covalency (DOC) of Transition Metal Sites. *Coord. Chem. Rev.* **2017**, *345*, 182−208.
(50) Groot, F. D. Multiplet Effects in X-Ray Spectroscopy. *Coord. Chem. Rev.* **2005**, *249*, 31−63.
(51) Czapla-Masztafiak, J.; Kubas, A.; Kayser, Y.; Fernandes, D. L. A.; Kwiatek, W. M.; Lipiec, E.; Deacon, G. B.; Al-Jorani, K.; Wood, B. R.; Szlachetko, J.; Sá, J. Mechanism of Hydrolysis of a Platinum(IV) Complex Discovered by Atomic Telemetry. *J. Inorg. Biochem.* **2018**, *187*, 56−61.
(52) Sá, J.; Czapla-Masztafiak, J.; Lipiec, E.; Kayser, Y.; Fernandes, D. L. A.; Szlachetko, J.; Dufrasne, F.; Berger, G. Resonant X-Ray Emission Spectroscopy of Platinum(II) Anticancer Complexes. *Analyst* **2016**, *141*, 1226−1232.
(53) Berger, G.; Fusaro, L.; Luhmer, M.; Czapla-masztafiak, J.; Lipiec, E.; Szlachetko, J.; Kayser, Y.; Fernandes, D. L. A.; Sá, J.; Dufrasne, F.; Bombard, S. Insights into the structure−activity relationships of chiral 1,2-diaminophenylalkane platinum(II) anticancer derivatives. *J. Biol. Inorg. Chem.* **2015**, *20*, 841−853.
(54) Lipiec, E.; Czapla, J.; Szlachetko, J.; Kayser, Y.; Kwiatek, W.; Wood, B.; Deacon, G. B.; Sá, J. Novel in Situ Methodology to Observe the Interactions of Chemotherapeutical Pt Drugs with DNA under Physiological Conditions. *Dalton Trans.* **2014**, *43*, 13839−13844.
(55) Milne, C. J.; Penfold, T. J.; Chergui, M. Recent Experimental and Theoretical Developments in Time-Resolved X-Ray Spectroscopies. *Coord. Chem. Rev.* **2014**, *277-278*, 44−68.
(56) Chen, L. X.; Zhang, X.; Shelby, M. L. Recent Advances on Ultrafast X-Ray Spectroscopy in the Chemical Sciences. *Chem. Sci.* **2014**, *5*, 4136−4152.
(57) Huynh, M. H. V.; White, P. S.; John, K. D.; Meyer, T. J. Isolation and Characterization of the Osmium(V) - Imido Complex [OsV(Tp)-(Cl)2(NH)]. *Angew. Chem., Int. Ed.* **2001**, *40*, 4049−4051.
(58) Maestri, A. G.; Cherry, K. S.; Toboni, J. J.; Brown, S. N. [4 + 1] Cycloadditions of Cyclohexadienes with Osmium Nitrides. *J. Am. Chem. Soc.* **2001**, *123*, 7459−7460.
(59) Huynh, M. H. V.; Meyer, T. J.; Labouriau, A.; Morris, D. E.; White, P. S.; Hill, C.; Carolina, N. Multiple Mixed-Valence Behavior in Reaction between Trans- [Os VI (Tpy)(Cl) 2 (N)] + and NH 3. *J. Am. Chem. Soc.* **2003**, *2*, 2828−2829.
(60) Man, W.-L.; Lam, W. W. Y.; Yiu, S.-M.; Lau, T.-C.; Peng, S.-M. Direct Aziridination of Alkenes by a Cationic (Salen)Ruthenium(VI) Nitrido Complex. *J. Am. Chem. Soc.* **2004**, *126*, 15336−15337.
(61) Man, W.-L.; Lam, W. W. Y.; Kwong, H.-K.; Peng, S.-M.; Wong, W.-T.; Lau, T.-C. Reaction of a (Salen)Ruthenium(VI) Nitrido Complex with Thiols. C-H Bond Activation by (Salen)Ruthenium(IV) Sulfilamido Species. *Inorg. Chem.* **2010**, *49*, 73−81.

https://doi.org/10.1021/acs.inorgchem.1c00467
Inorg. Chem. 2021, 60, 6663−6671

(62) Thom, A. J. W.; Sundstrom, E. J.; Head-Gordon, M. LOBA: A Localized Orbital Bonding Analysis to Calculate Oxidation States, with Application to a Model Water Oxidation Catalyst. *Phys. Chem. Chem. Phys.* **2009**, *11*, 11297−11304.
(63) Kurian, R.; Van Schooneveld, M. M.; Zoltán, N.; Vankó, G.; De Groot, F. M. F. Temperature-Dependent 1s2p Resonant Inelastic X-Ray Scattering of CoO. *J. Phys. Chem. C* **2013**, *117*, 2976−2981.
(64) Hirsch, O.; Kvashnina, K. O.; Luo, L.; Süess, M. J.; Glatzel, P.; Koziej, D. High-Energy Resolution X-Ray Absorption and Emission Spectroscopy Reveals Insight into Unique Selectivity of La-Based Nanoparticles for CO2. *Proc. Natl. Acad. Sci. U. S. A.* **2015**, *112*, 15803−15808.
(65) Williams, D. S.; Coia, G.; Meyer, T. Trans-Cis Isomerization in [Os(Tpy)(C1)2(N)]+. *Inorg. Chem.* **1995**, *34*, 586−592.
(66) Suntharalingam, K.; Johnstone, T. C.; Bruno, P. M.; Lin, W.; Hemann, M. T.; Lippard, S. J. Bidentate Ligands on Osmium(VI) Nitrido Complexes Control Intracellular Targeting and Cell Death Pathways. *J. Am. Chem. Soc.* **2013**, *135*, 14060−14063.
(67) Pedersen, K. S.; Woodruff, D. N.; Singh, S. K.; Tressaud, A.; Durand, E.; Atanasov, M.; Perlepe, P.; Ollefs, K.; Wilhelm, F.; Mathonière, C.; Neese, F.; Rogalev, A.; Bendix, J.; Clérac, R. [OsF6]X−: Molecular Models for Spin-Orbit Entangled Phenomena. *Chem. - A Eur. J.* **2017**, *23*, 11244−11248.
(68) Szlachetko, J.; Nachtegaal, M.; de Boni, E.; Willimann, M.; Safonova, O.; Sa, J.; Smolentsev, G.; Szlachetko, M.; van Bokhoven, J. A.; Dousse, J.-C.; Hoszowska, J.; Kayser, Y.; Jagodzinski, P.; Bergamaschi, A.; Schmitt, B.; David, C.; Lücke, A. A von Hamos X-Ray Spectrometer Based on a Segmented-Type Diffraction Crystal for Single-Shot x-Ray Emission Spectroscopy and Time-Resolved Resonant Inelastic x-Ray Scattering Studies. *Rev. Sci. Instrum.* **2012**, *83*, 103105.
(69) Tulkki, J.; Aberg, T. Behaviour of Raman Resonance Scattering across the K X-Ray Absorption Edge. *J. Phys. B At. Mol. Phys.* **1982**, *15*, L435.
(70) Deslattes, R. D.; Kessler, E. G.; Indelicato, P.; De Billy, L.; Lindroth, E.; Anton, J. X-Ray Transition Energies: New Approach to a Comprehensive Evaluation. *Rev. Mod. Phys.* **2003**, *75*, 35−99.
(71) Campbell, J. L.; Papp, T. Atomic Level Widths for X-Ray Spectrometry. *X-Ray Spectrom.* **1995**, *24*, 307−319.
(72) Rehr, J. J.; Kas, J. J.; Vila, F. D.; Prange, M. P.; Jorissen, K. Parameter-Free Calculations of X-Ray Spectra with FEFF9. *Phys. Chem. Chem. Phys.* **2010**, *12*, 5503.
(73) Neese, F. The ORCA Program System. *Wiley Interdiscip. Rev. - Comput. Mol. Sci.* **2011**, *2*, 73−78.
(74) Chai, J.-D.; Head-Gordon, M. Long-Range Corrected Hybrid Density Functionals with Damped Atom-Atom Dispersion Corrections. *Phys. Chem. Chem. Phys.* **2008**, *10*, 6615−6620.
(75) Weigend, F.; Ahlrichs, R. Balanced Basis Sets of Split Valence, Triple Zeta Valence and Quadruple Zeta Valence Quality for H to Rn: Design and Assessment of Accuracy W. *Phys. Chem. Chem. Phys.* **2005**, *7*, 3297−3305.
(76) Weigend, F. Accurate Coulomb-Fitting Basis Sets for H to Rn. *Phys. Chem. Chem. Phys.* **2006**, *8*, 1057−1065.
(77) Van Lenthe, E.; Baerends, E. J.; Snijders, J. G. Relativistic Regular Two-Component Hamiltonians. *J. Chem. Phys.* **1993**, *99*, 4597.
(78) Peng, C.; Bernhard, H. S. Combining Synchronous Transit and Quasi-Newton Methods to Find Transition States. *Isr. J. Chem.* **1993**, 449−454.
(79) Peng, C.; Ayala, P. Y.; Schlegel, H. B.; Frisch, M. J. Using Redundant Internal Coordinates to Optimize Equilibrium Geometries and Transition States. *J. Comput. Chem.* **1996**, *17*, 49−56.
(80) Tomasi, J.; Mennucci, B.; Cammi, R. Quantum Mechanical Continuum Solvation Models. *Chem. Rev.* **2005**, *105*, 2999−3094.
(81) Glendening, E. D.; Badenhoop, J. K.; Reed, A. E.; Carpenter, J. E.; Bohmann, J. A.; Morales, C. M.; Landis, C. R.; Weinhold, F. NBO 6.0. *Theor. Chem. Institute,* Univ. Wisconsin: Madison, WI 2013.

https://doi.org/10.1021/acs.inorgchem.1c00467
Inorg. Chem. 2021, 60, 6663−6671